2021

Computational Fluid Dynamics Study on Transonic Axial Compressors using Cartesian Cut-Cell Based Method with Adaptive Mesh Refinement and Boundary Layer Mesh

Yanheng Li
Convergent Science Inc., United States of America, yanheng.li@convergecfd.com

David Henry Rowinski

Karthik Rudra Reddy

Karan Bansal

Computational Fluid Dynamics Study on Transonic Axial Compressors using Cartesian Cut-Cell Based Method with Adaptive Mesh Refinement and Boundary Layer Mesh

Yanheng LI*, David Henry ROWINSKI*, Karthik RUDRA REDD, Karan BANSAL,
Convergent Science Inc.,
Madison, Wisconsin, United States

Contact Information (+1-608-230-1552, yanheng.li@convergecfd.com,
david.rowinski@convergecfd.com)

* Corresponding Author

ABSTRACT

Axial compressors are used extensively in the energy, power, and transportation industries. Computational Fluid Dynamics (CFD) has been widely used in research and development of dynamic compressors. CFD modeling for such designs often presents great challenges in terms of meshing and computational cost due to moving parts with complex shapes, tiny gaps, and a large range of length scales and time scales to resolve. In this work, a Cartesian cut-cell based method with adaptive mesh refinement (AMR) is used to study Rotor 67, a transonic axial compressor design from NASA. The adopted method is demonstrated to be easily implemented and copmutationally efficient through a mesh convergence study, largely due to the advantage of an autonomously generated Cartesian cut-cell grid and AMR. Additionally, a boundary layer mesh can be used in conjunction with the Cartesian cut-cell mesh in order to resolve the near-wall flow more efficiently. Both the frozen-rotor approach with a single non-inertial reference frame (SRF) and a moving-rotor approach in a single inertial reference frame are used for the computation of the global pressure ratio and the isentropic efficiency as well as the local flow velocity, pressure, and temperature. Results show great grid convergence and good agreement with previously published experimental data for multiple operating conditions in terms of both global and local flow quantities.

1. INTRODUCTION

Axial compressors are an important type of dynamic compressor and have a wide variety of applications in the energy, power generation, and transportation industries due to their advantages of being able to accommodate a high volumetric flow rate, high efficiency, smoothness, and ease in multi-stage operation. Computational Fluid Dynamics (CFD) has been used extensively in the modeling and design of axial compressors, from global performance evaluations to studies of local flow details. However, complex curvature of the geometries, high rotational speeds, and tiny tip clearances often create great challenges for CFD meshing and often incurs a conservation/stability issue for the numerical solution: the cells are often skewed with poor aspect ratios near the complex locations and the conservation of volume is difficult. The meshing for such designs is often time-consuming with difficulties in assuring the mesh quality, which consequently affects the numerical performance of a CFD solution.

There are many existing efforts on computational modeling of the flow dynamics of an axial compressor. Grosvenor (2008) studied the NASA Rotor 67 transonic axial compressor using the Jameson-Schmidt-Turkel (JST) scheme and the Spallart-Allmaras turbulence modeling with a body-fitted mesh and compared against the original test data. Conelius et. al. (2014) employed both a transient and a steady-state solver to study multi-stage axial compressors with an unstructured mesh. Charalambous et. al. (2004) used a similar methodology and tools to study the effect of the inflow distortion on compressor performance. Most of the exiting studies require a dedicated user-created mesh with professional or commercial mesh generation tools, which typically involves long time and a recursiverevision process without precise knowledge beforehand on where the mesh should be further refined to capture the flow physics more accurately. Moreover, for different operating conditions, the flow could vary considerably, and the mesh may need

appropriate adjustments which further increase the time cost in creating a mesh suitable for a wide variety of operating conditions of an axial compressor. A grid convergence study could require additional meshing time to investigate the uncertainty due to different grid resolution, which is an essential part of any detailed CFD study.

In this study, a Cartesian cut-cell method is used to investigate the NASA Rotor 67 transonic axial compressor characterized in Strazisar (1989). A single non-inertial reference frame (SRF) is used for most of the design performance studies and comparison with test data. This study features a novel autonomous meshing method which automatically generates a Cartesian mesh on-the-fly to fill the original triangulated surface geometry without requiring any user meshing time. At the locations where a Cartesian cell meets the boundary, the cell is cut to fit the boundary geometry exactly, without the need to distort the original boundary geometry, hence perfectly conserving the domain volume. Based on the gradient or curvature of the velocity and temperature fields, the grid is dynamically refined through adaptive mesh refinement (AMR), without requiring any a-priori knowledge of the flow field. The total pressure rise, adiabatic efficiency, and local flow details at the impeller exit have been studied and compared with the experiment data, with a reasonable match and good grid convergence. It is demonstrated that, although most of these studies are performed using a single blade passage sector geometry in a SRF and with a steady-state solver for computational efficiency, the same problem is also solved using the moving full geometry to conduct transient behavior studies, which renders this methodology tractable for industrial problems in which the assumptions of such geometry simplifications may not be practical. In addition, the adopted meshing technique can be optionally combined with body-fitted boundary layer mesh to resolve the near-wall and gap flow details with higher accuracy. Similar approaches have been successfully applied for several similar pump and compressor studies, including screw compressors, reciprocating compressors [Rowinski (2016)], and centrifugal fans [Li(2018)].

2. TEST CASE AND METHODOLOGY

The NASA Rotor 67 model is a single stage transonic axial compressor, originally built and experimentally tested in 1989 at the NASA Glenn Research Center [Strazisar (1989)]. It has 22 back-swept blades, with a converging cross-sectional area from the inlet to the outlet (Figure 1). The test rig has a standard test condition of the inlet total air temperature at 288.15K and total pressure of 1 atm (101325Pa). At the tested speed of 16,043 revolutions per minute, the impeller tip speed is 429 m/s with a Mach number of 1.38. A single self-nulling combination probe wase used for measuring total pressure, total temperature, and flow angle, while single self-nulling 18-degree wedge-angle probes were used for static pressure measurement. The velocity was measured by laser anemometer. Most of the presented studies focus on the steady state result, hence a sector geometry is used for computational efficiency, and both a standard model with a tip clearance of 0.61mm and a model with zero tip clearance are investigated. The full moving geometry is demonstrated to be useful for further transient studies and yields steady-state results consistent with the sector model. Both geometries are based on the study from [Doi (2002)].

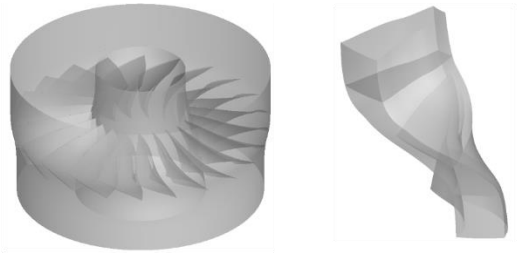

Figure 1: Rotor 67 full geometry (left) and sector geometry with a single blade passage (right).

The commercial code CONVERGE [(Richards et. al. (2017)] is used for the study, which adopts a second-order finite volume scheme with the aforementioned Cartesian cut-cell grid, originally proposed by Senecal et. al. (2007). The governing momentum, energy and turbulence transport equations are solved on a finite-volume grid with all quantities collocated at the cell center. The Pressure Implicit with Splitting of Operators (PISO) method [Issa (1985)] is used for pressure-velocity coupling. Since the Cartesian cells may be cut by the wall boundary, to ensure a good aspect ratio and sufficient cell volume, small cut-cells will be merged with nearby full cells in a technique termed cell-pairing, the

degree to which can be controlled by a single parameter termed the minimum volume ratio. In this study, a value of 0.3 is used for this parameter, which means that if a ratio of a cut-cell's volume to its volume before being cut is less than 0.3, it will be paired to the neighboring cell with which it shares the most volume. The cell-pairing scheme can further improve the numerical stability on the basis of Cartesian cut-cell grid's overall good orthogonality and perfect aspect ratio. Automatic and variable time step control is used based on Courant-Friedrichs-Lewy (CFL) numbers. Message Passing Interface (MPI) and shared memory are used for parallelization. Automatic Mesh Refinement (AMR) is employed to adaptively refine the mesh based on local variations of velocity and temperature to efficiently refine the mesh around the locations where the flow is most sensitive (for example, at the shock wave across the blade tip) for a highly-efficient mesh for a wide range of operating conditions as demonstrated in Pomraning(2014). A typical overview of the Cartesian cut-cell grid system is shown in Figure 2.

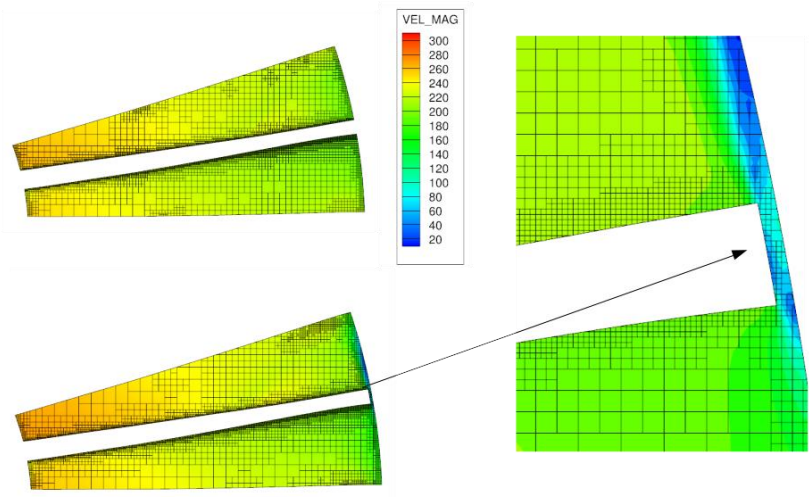

Figure 2: The Cartesian cut-cell grid system for zero tip clearance model (left upper) and for the model with a 0.61 mm tip gap (left lower and right).

A compressible gas solver is used with the ideal gas as equation of state. To avoid the common checker-boarding issue for collocated cells, the scheme from Rhie and Chow (1983) is used with the pressure-velocity coupling methodology. Due to the high velocities and prominent turbulent flow features in these cases, the Reynolds Averaged Navier-Stokes (RANS) equations are used for turbulence modeling. Most cases in this work are run with the Reynold-Stress Model (RSM) RANS turbulence modeling [Liu et. al. (2020)] except in cases specifically mentioned. The RSM model, involves seven additional transport equations for turbulent kinetic energy, dissipation rate, and the individual components of the Reynolds stress tensor, and has shown good applicability in rotating flows. For meshes with finer resolution (y+<30), the Shear Sress Transport (SST-k-Omega) RANS model from Menter (1994) is used instead. The transport equations are solved by the Successive Over-Relaxation (SOR) algorithm. At the wall boundaries, standard law-of-the-wall models are used for velocity for RSM turbulence model and automatic wall functions are used for SST turbulence model. The inlet is set at 1 atm of total pressure according to the test condition, and different outflow static pressures are prescribed according to the multiple test conditions. A steady state solver is used for most of the studies, with the exception of the moving full geometry case.

3. Results and Discussion

3.1 Global Performance Predictions

For the baseline runs, a 5 mm base grid is used with maximum level of refinement of 4, corresponding with the minimum grid size of $5/2^4$=0.3125 mm and an average y+ around 30 near the pressure side of the blade and a maximum cell count of 1.62M cells. The maximum CFL number is set at 10, but it will reduce to 1 at the final stage of each run, which corresponds to a time step range within 2e-7s to 2e-6s. A single condition can be run to a steady state within 12 hours with 16 CPUs. According to the original test, the pressure ratios are based on the total pressure measured at

station 1 (impeller inlet at z=2.743cm) and station 2 (impeller exit at z=-11.011cm). The adiabatic efficiency is calculated based on equation (1).

$$\eta = \frac{\left(\frac{p_{t2}}{p_{t1}}\right)^{\frac{\gamma-1}{\gamma}} - 1}{\frac{T_{t2}}{T_{t1}} - 1}, \qquad (1)$$

Where p_t is the total pressure, T_t is the total temperature, γ is the heat capacity ratio (1.4 for dry air). Subscripts 1 and 2 denote station 1 and station 2, respectively. With the baseline setup and RSM RANS turbulence model, the model performance is compared against test data in Figure 3.

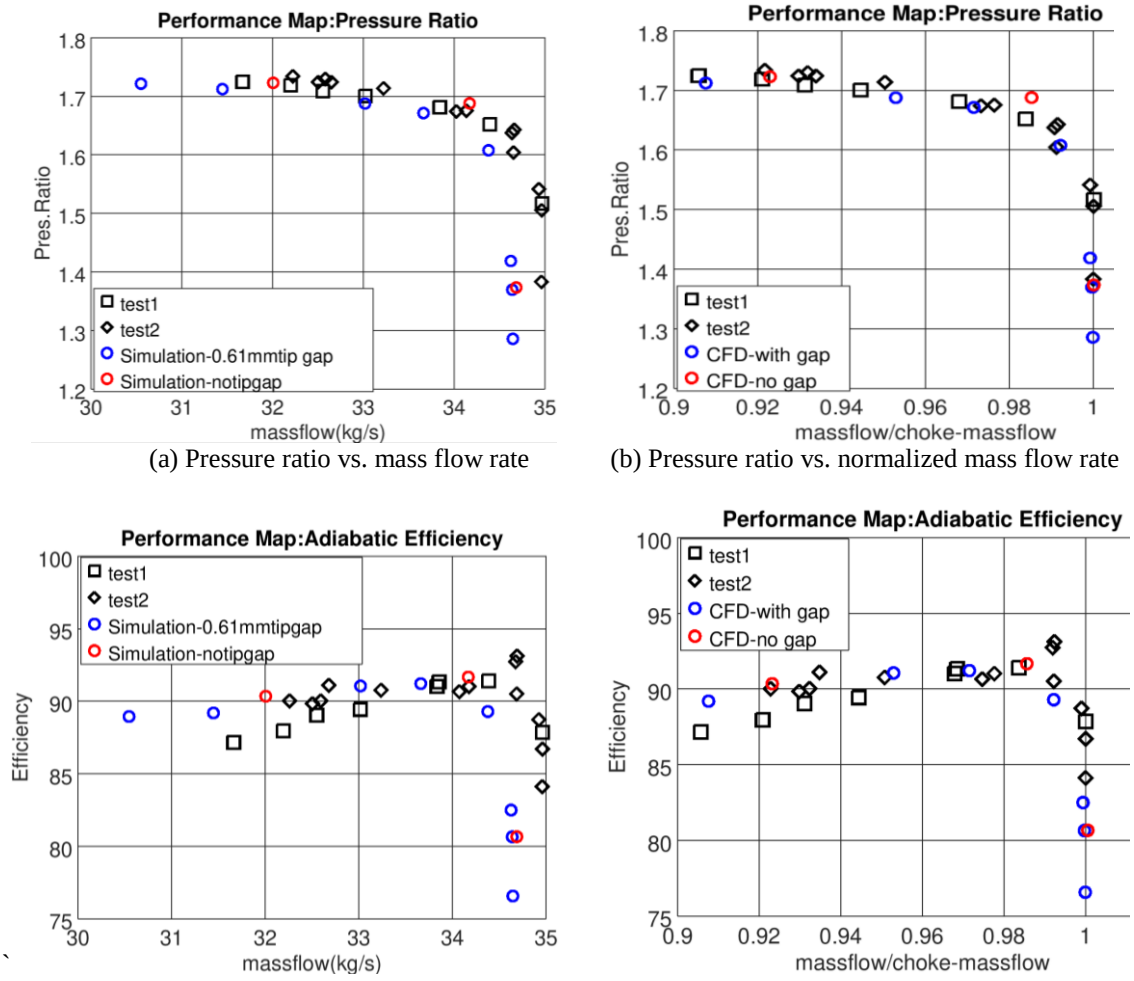

(a) Pressure ratio vs. mass flow rate (b) Pressure ratio vs. normalized mass flow rate

(c) Adiabatic Efficiency vs. mass flow rate (d) Adiabatic efficiency vs. normalized mass flow rate

Figure 3: Pressure ratio and Adiabatic Efficiency vs. mass flow rate.

From figures 3(a) and 3(c) illustrate that the overall trends of both pressure ratio and the efficiency curve are well matched against the measured test data, with the predicted choke mass flow rate of 34.70 kg/s within 1% of the 34.96 kg/s test data. For most of existing studies, the dimensionless mass flow normalized by the predicted choke mass flow is often used as a metric for comparison [Grosvenor (2008)]. Therefore, the normalized pressure ratio and efficiency curve are also shown in Figures 3(b) and 3(d), respectively. The normalized curve indicates that the peak efficiency location and the near stall condition match well with the test data. The leakage effect of the tip clearance can be

observed when comparing the previous results to the results from the cases without tip gap. The tip gap results in overall slight lower performance due to the additional leakage loss.

In CFD studies on dynamic compressors, numerical error from the grid resolution is a common issue that needs to be carefully addressed. For this work, the choke mass flow rate is an important quantity to be used in normalization, and it ought to demonstrate good grid convergence or low grid uncertainty. Figure 4 shows the grid dependency of the choke mass flow rate on five grids of varying resolution, whose y+ values range from 100 on grid 0 to 30 on grid 4, considering the average on the pressure side of the blade. Good grid convergence can be observed, and most of the studies in this work utilize grid 4. The adopted Cartesian cut-cell meshing approach allows a global grid convergence study to be performed easily and robustly, simply by changing the base grid size and optionally the maximum level of refinement in AMR.

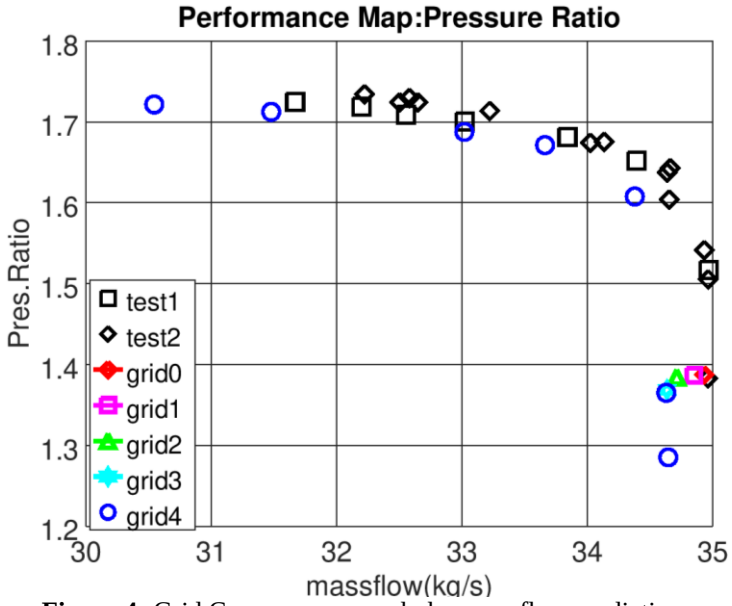

Figure 4: Grid Convergence on choke mass flow prediction.

3.2 Predictions of Local Flow Details

To further validate the proposed method, the local flow details for the near-peak and near-stall condition are also assessed in this work for the model including the gap clearance. In the original experiment, the radial distribution of total pressure, total temperature, static pressure and flow angle are presented for both a near-stall condition (corresponding to a total pressure ratio of 1.728) and a near-peak condition (corresponding to a total pressure ratio of 1.642) at station 2. Since in this work the static pressure boundary condition is used at the outlet, the results from two conditions closest to the test condition (with less than 1% difference in total pressure ratio) are averaged. The comparisons are shown in Figure 5.

Figure 5 shows that even at the relatively coarse resolutions (where the y+ is around 30) used as the baseline setup, the prediction of pressure and temperature distribution at impeller exit matches reasonably well with the test data for both the near-peak and near-stall conditions. The results also suggest that the ideal gas law used for the equation of state is sufficiently accurate for the dry air at the given condition, and that there is no need to choose a more advanced equation of state for these conditions (which would otherwise increase the computational cost slightly and make the adiabatic efficiency used in Eq. (1) less precise). As for the flow angle (defined as the angle between the flow direction and velocity component normal to the flow), there is overall around 4 degrees of difference compared with test data, but the minimum angle radial positions are accurately captured compared with the test data. The overall validation shown in Figures 3, 4 and 5 demonstrate the validity of the proposed methodology. The static temperature, static pressure and velocity contours at the middle axial chord (z=-4.62cm) are shown in Figure 6 for near-stall, near-peak, and near-choke conditions using the same color scale for each quantity. The shock wave which starts forming from choke to peak at the pressure side, and then shifting to the suction side, is clearly evident in these contour plots.

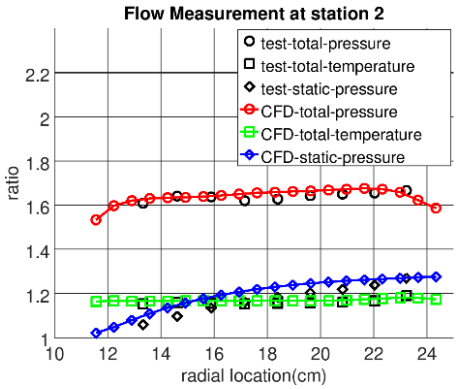

(a) pressure/temperature-near peak

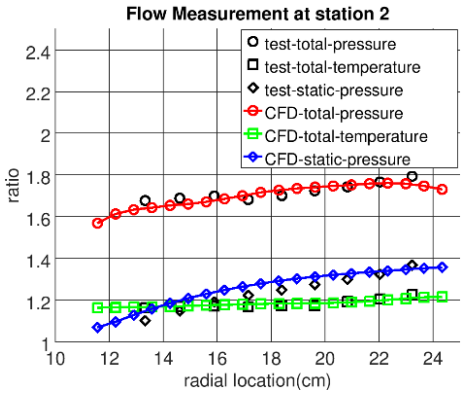

(b) pressure/temperature-near stall

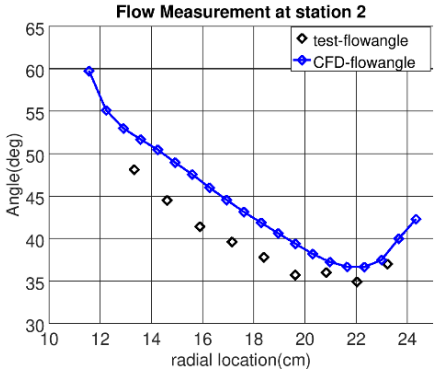

(c) flow angle-near peak

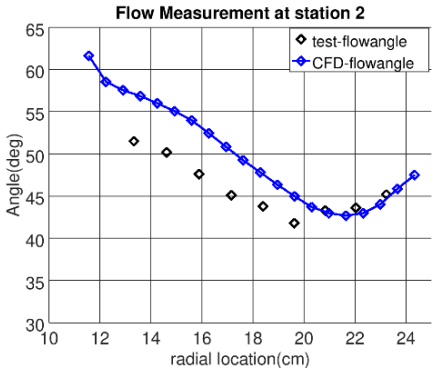

(d) flow angle-near stall

Figure 5: Radial distriubtion of flow measurement compared with test.

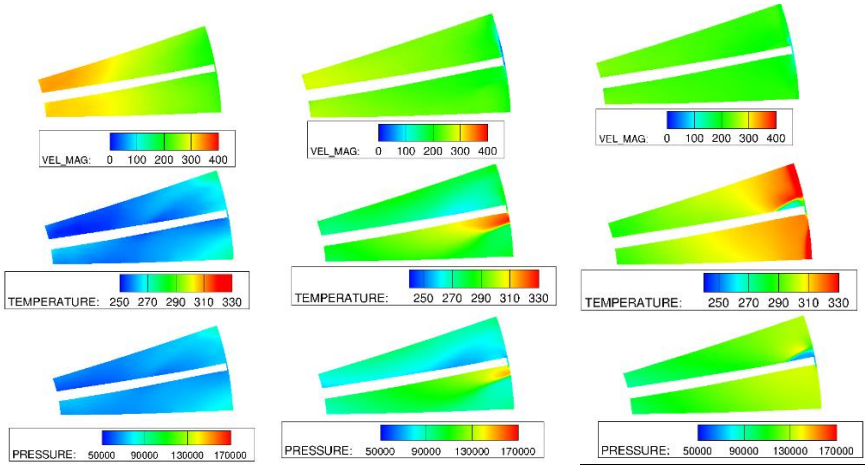

(a) near-choke (b) near-peak (c) near-stall

Figure 6: Flow field comparison at different conditions at middle axial chord.

3.3 Other Investigations and Future Work

For the above studies of the global and local flow fields, the sector geometry is used for computational efficiency. It is necessary to verify that the sector geometry and non-inertial reference frame are an accurate compared to the actual full moving geometry. Two coarse grid runs (with y+ values around 100, base grid sizes of 8 mm, and minimum grid sizes of 1 mm), one with a sector geometry and one with full moving geometry, are set up in exactly the same way and run side-by-side for the near-peak condition . The full moving geometry has a total cell count of 12M cells while the sector geometry has a total cell count of 0.5M cells. The pressure and velocity contours at the mid chord (z=-

4.5cm) location are presented as Figure 7. From the comparison, it is evident that the axisymmetry of the flow field is sufficient to justify the choice of a sector geometry, and for these models and conditions, there is very little blade to blade variation in flow quantities. Although with all Cartesian grids, there may be slight numerical effects due to the sector geometry alignment angle with the orthogonal direction of the grid. Different grid alignments may cause slight resolution change near the wall, while the full moving geometry does not have such an issue.

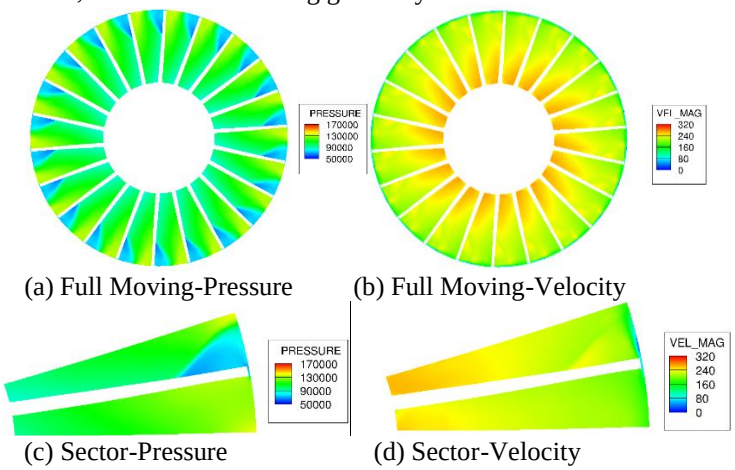

Figure 7: Comparison between full moving geometry and sector geometry run at near peak condition.

Finally, if detailed vortex structures near the wall and the gap are of specific interest, further grid refinement is needed than the current y+ levels of 30, at which point the structured Cartesian grid may become less efficient as the body-fitted boundary layer mesh for the curved surface of an axial compressor. The proposed numerical scheme allows a hybrid scheme: the user can create a boundary layer mesh for the blade before the simulation, and for the remaining majority of the domain, a Cartesian cut-cell will still be automatically created on-the-fly. The interface between the Cartesian cut-cell and the boundary layer mesh will be handled automatically by the proposed methodology during run time as shown in Figure 8. With the help of this hybrid meshing strategy, a fine resolution of 6E-6m and y+ values less than 2 (compared with the 0.625mm finest resolution for the Cartesian cut-cell baseline setup) can be achieved while still maintaining similar base Cartesian cut-cell resolution level and allowing the AMR to resolve the shock. The total cell count only increased from 1.6M cells to 3M cells, making the overall run time still within an acceptable level. It can be seen from the pressure contour in Figure 8 that more small scale flow details are captured with the help of the finer resolution.

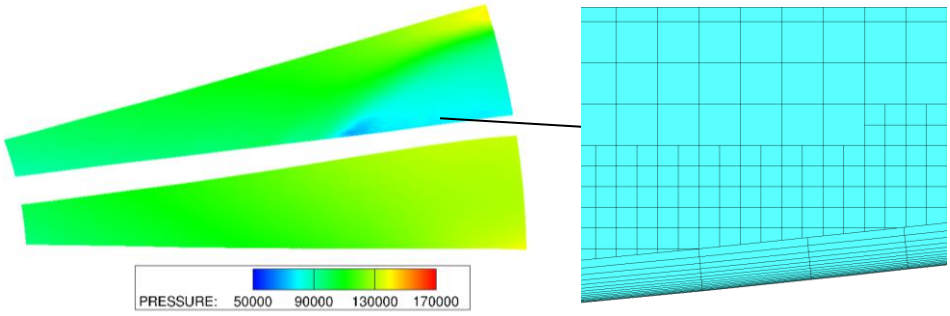

Figure 8: Hybrid mesh near blade and the pressure field.

4. CONCLUSIONS

This work presents a CFD modeling study of an axial compressor design (NASA Rotor 67) using an automated Cartesian cut-cell based finite-volume method with optional hybrid boundary-layer mesh. The employed method largely eliminates mesh-related user time and instability/numerical diffusion due to poor mesh quality. It offers the advantage of easily performed grid convergence studies and multi-condition study of the design. With the help of

adaptive mesh refinement, the computational efficiency is further enhanced without the need to know the flow field before the simulation for a grid strategy that performs efficiently across a variety of operating conditions.

Global flow quantities are compared against the original test data for total pressure ratio and adiabatic efficiency as functions of mass flow rate, and demonstrated good agreement across the full operation range. This includes the predictions for choke mass flow rate, the peak efficiency location, and overall near stall performance. Grid convergence trends have been clearly observed with the chosen grid resolutions. For the local flow quantities, the radial distribution of total pressure, static pressure, total temperature and flow angle at the impeller exit are studied and validated against test data, with reasonable match in the average value, extreme value locations, and overall trends at both near-stall and near-peak conditions. These validations justify the choice of the grid resolution, the RSM RANS turbulence model, and the overall solution scheme. The mid-chord velocity, pressure, and temperature contours are shown to illustrate how the shock wave is generated and shifts from the pressure side to the suction side when the condition changes from near-choke to near-peak and to near-stall. Moreover, a comparison between the sector geometry and the full moving geometry result at the mid-chord proves the validity of using a sector geometry for the steady state study since the observed flow field is quite axisymmetric for the studied model and operation conditions.

Finally, although the all Cartesian cut-cell grid strategy can theoretically handle any type of geometry, it is not as efficient in fully resolving the boundary layer of an axial compressor blade surface which is curved and not necessarily aligned with the grid line direction. A hybrid meshing strategy can be used to solve this problem, which requires the user provide the boundary-layer mesh before the simulation while the Cartesian cut-cell grid will be created on-the-fly for remaining part of the domain. The two mesh interfaces will be automatically handled by the proposed method. With this hybrid meshing approach, a similar grid resolution for the location far from the boundary is maintained, while utilizing a boundary-layer mesh to fully and efficiently resolve the near wall effect and allowing AMR to efficiently resolve the shock wave.

REFERENCES

Charalambous, Nikolaos, et al. "Axial compressor response to inlet flow distortions by a CFD analysis." *Turbo Expo: Power for Land, Sea, and Air*. Vol. 41707. 2004.

Cornelius, Christian, et al. "Experimental and computational analysis of a multistage axial compressor including stall prediction by steady and transient CFD methods." *Journal of Turbomachinery* 136.6 (2014).

Doi, H. and Alonso, J.J., "Fluid/Structure Coupled Aeroelastic Computations for Transonic Flows in Turbomachinery", ASME Turbo Expo 2002, GT-2002-30313, Amsterdam, the Netherlands, June 3-6, 2002.

Grosvenor, A. D. 2008. Numerical studies toward prediction, analysis and treatment of SWBLI in transonic compressors. 14th Conference (International) on the Methods of Aerophysical Research Proceedings. Section 2. Novosibirsk, Russia. CD. ISBN 978-5-98901-040-0. 10 p.

Issa, R. I. (1985). Solution of the Implicitly Discretised Fluid Flow Equations by Operator-Splitting. *Journal of Computational Physics*, 62.

Li, Y., Rowinski, H.D., Bansal, K., & Reddy, R.K., CFD modeling and performance evaluation of a centrifugal fan using a cut-cell method with automatic mesh generation and adaptive mesh refinement, International Compressor Engineering Conference, 2018.

Liu, Z., Wijeyakulasuriya, S., Mashayekh, A., and Chai, X., "Investigation of Reynolds Stress Model for Complex Flow Using CONVERGE," SAE Technical Paper 2020-01-1104, 2020, https://doi.org/10.4271/2020-01-1104.

Menter, F.R., (1994), Two-equation eddy-viscosity turbulence models for engineering applications. AIAA-Journal, 32(8), pp. 269-289, 1994.

Pomraning, E., Richards, K., and Senecal, P. (2014). Modeling Turbulent Combustion Using a RANS Model, Detailed Chemistry, and Adaptive Mesh Refinement. *SAE Technical Paper 2014-01-1116.*

Rhie, C. M. and Chow, W. L. (1983). Numerical Study of the Turbulent Flow Past an Airfoil with Trailing Edge Separation.AIAA J., 21, 1525-1532.

Richards, K. J., Senecal, P. K., Pomraning, E. (2017). CONVERGE 2.4 Manual, Convergent Science Inc., Madison, WI.

Rowinski, D. H. and Davis, K. E. (2016). Modleing Reciprocating Compressors Using A Cartesian Cut-Cell Method With Automatic Mesh Generation. International Compressor Engineering Conference (2016).

Senecal, P. K., Pomraning, E., Richards, K. J., Briggs, T. E., Choi, C. Y., McDavid, R. M., Patterson, M. A., Hou, S., & Shethaji, T. (2007). A New Parallel Cut-Cell Cartesian CFD Code for Rapid Grid Generation Applied to In-Cylinder Diesel Engine Simulations. SAE Technical Paper, #2007-01-0159.

Strazisar, A.J., Wood, J.R., Hathaway, M.D., Suder, K.L., 1989, "Laser Anemometer Measurements in a Transonic Axial-Flow Fan Rotor," NASA TP-2879.